

Mitotic Golgi is in a Dynamic Equilibrium Between Clustered and Free Vesicles Independent of the ER

Stephen A. Jesch*, Amy J. Mehta*,
Meel Velliste¹, Robert F. Murphy and
Adam D. Linstedt**

Department of Biological Sciences and ¹Program in
Biomedical & Health Engineering, Carnegie Mellon
University, Pittsburgh, PA 15213, USA

**Corresponding author: Adam D. Linstedt,
linstedt@andrew.cmu.edu

Golgi inheritance during cell division involves Golgi disassembly but it remains unclear whether the breakdown product is dispersed vesicles, clusters of vesicles or a fused ER/Golgi network. Evidence against the fused ER/Golgi hypothesis was previously obtained from subcellular fractionation studies, but left concerns about the means used to obtain and disrupt mitotic cells. Here, we performed velocity gradient analysis on otherwise untreated cells shaken from plates 9 h after release from an S-phase block. In addition, we used digitonin and freeze/thaw permeabilization as alternatives to mechanical homogenization. Under each of these conditions, approximately 75% of the Golgi was recovered in a population of small vesicles that lacked detectable ER. We also used multilabel fluorescent microscopy with optical sectioning by deconvolution to compare the 3D metaphase staining pattern of endogenous Golgi and ER markers. Although both ER and Golgi staining were primarily diffuse, only the ER was excluded from the mitotic spindle region. Surprisingly, only 2% of the Golgi fluorescence was present as resolvable structures previously characterized as vesicle clusters. These were not present in the ER pattern. Significantly, a portion of the diffuse Golgi fluorescence, presumably representing dispersed 60-nm vesicles, underwent an apparent rapid aggregation with the larger Golgi structures upon treatments that impaired microtubule integrity. Therefore, mitotic Golgi appears to be in a dynamic equilibrium between clustered and free vesicles, and accurate partitioning may be facilitated by microtubule-based motors acting on the clusters to insure random and uniform distribution of the vesicles.

Key words: ER, Golgi, mitosis, partitioning, vesicles

Received 11 July 2001, revised and accepted for publication 14 August 2001

The interphase Golgi mediates the processing and sorting of newly synthesized proteins and lipids. It may also participate in other important cellular reactions including certain signaling pathways (1). These essential roles argue that mechanisms exist to insure Golgi inheritance by each daughter during cell division. Indeed, the accuracy of Golgi partitioning, as determined from the distribution of a fluorescently labeled Golgi marker in telophase HeLa cells, is close to perfect (2). Although our understanding of the mechanism that achieves this inheritance is incomplete, it is clear that it involves a dramatic rearrangement of interphase Golgi structure.

The interphase Golgi consists of mostly interconnected stacked membranes, usually positioned near the centrosome. The integrity and growth of the Golgi depends on a proper balance of incoming and outgoing membrane flow. Membrane input and output, mediated in large part by transport vesicles, occurs at both ends of the stack, and transport within the stack is also bi-directional (3). Most of the forward traffic corresponds to the movement of newly synthesized material to, through, and out of the Golgi. The backward traffic largely mediates the retrieval of escaped secretory pathway residents to maintain their proper localization. The stacked structure of the Golgi probably serves to increase the efficiency of vesicle transport and also reflects an underlying process of progressive cisternal maturation (4). Efficiency of transport may also be aided by the positioning of the Golgi near microtubule minus-ends as it allows incoming membranes to be directed to the Golgi by the minus-end directed microtubule motor cytoplasmic dynein. In fact, Golgi position itself depends on dynein activity as well as an intact microtubule network (5).

As cells pass the G2/M boundary of the cell cycle, the activation of protein kinases leads to breakdown and dispersal of interphase Golgi structure (6–8). Although the key substrates of these kinases are unknown, part of the reaction involves disruption of microtubule-dependent Golgi positioning. This is a consequence of the dramatic rearrangement of the microtubules themselves en route to mitotic spindle formation and also of mitotic inhibition of cytoplasmic dynein (9). Another part involves the arrest of membrane traffic into, but not out of the Golgi. Recruitment of the COPII protein complex to the ER membrane for ER export is blocked in mitotic cells (10,11). Also, binding of p115, a vesicle docking protein required for ER to Golgi transport, to at least one of its membrane receptor complexes, GM130/GRASP65, is inhibited by mitotic phosphorylation of GM130 (12). In contrast, localization of the COPI coat to Golgi membranes is not affected and COPI vesicle formation from the Golgi is sup-

*These authors contributed equally.

ported in mitotic cytosol (13). Because p115 also mediates docking of Golgi-derived COPI vesicles (14), the inhibition of p115/GM130/GRASP65 complex formation may cause COPI vesicle accumulation at the expense of the Golgi. On the other hand, nocodazole-induced microtubule disruption in interphase cells is followed by Golgi redistribution to peripheral sites via the ER (15–18). Due to the ER export block, this same reaction at M-phase may cause Golgi redistribution to the ER, presumably by a COPI-independent pathway such as that mediated by rab6 (19). Thus, breakdown mechanisms may be in place for both Golgi vesiculation and Golgi-to-ER redistribution, and the extent to which either is involved would be reflected by Golgi protein localization at the completion of disassembly. Golgi disassembly is essentially complete by metaphase and it is the disassembled Golgi that is accurately partitioned during cell division (20,21).

What is needed therefore is an accurate picture of the state of the disassembled metaphase Golgi. Currently this is controversial. One view is that mitotic Golgi is present as a large number of uniformly dispersed vesicles and a lesser number of incompletely broken down fragments termed vesicle clusters and/or cisternal remnants (22–24). Because of the large number of elements, accurate inheritance can be accounted for by a mechanism that simply insures uniform dispersal of these elements at the time of division (25). Another view is that the Golgi is present as approximately 130 tubulo-vesicular clusters (2). Because of the small number of Golgi elements, the accurate inheritance of the Golgi cannot be accounted for by a mechanism that insures uniform dispersal. Instead, some sort of mechanism that actively segregates Golgi elements must be assumed to be present. Spindle microtubules might be involved as the Golgi tubulo-vesicular elements are observed in apparent association with spindle microtubules (20). A final view is that Golgi proteins and lipids are uniformly dispersed throughout the ER (21). Inheritance of the Golgi would depend on accurate partitioning of the ER. The mechanisms that account for ER partitioning are unknown, but because the organelle appears dispersed in a reticulum throughout most of the interior of dividing cells it is likely that inheritance can be achieved as long as a uniform dispersal of the membranes and their contents is maintained.

The view that the Golgi redistributes into the ER during division clearly predicts that mitotic Golgi and ER membranes cannot be separated from one another and that mitotic Golgi and ER marker staining should extensively colocalize. In contrast to these predictions, we previously reported that approximately 75% of the Golgi is present in dispersed small vesicles that are readily separated from the ER by velocity gradient sedimentation (24). The validity of this result has been questioned as the experiments involved nocodazole-arrested mitotic cells (26,27). Therefore, in this report we have carried out our subcellular fractionation on normally cycling mitotic cells. In addition, we have carried out a 3D immunofluorescence analysis of metaphase cells to test for differences between ER and Golgi patterns and to test

whether mitotic Golgi clusters, if present, represent the major form of the mitotic Golgi. As before, we have used endogenous Golgi and ER markers to avoid mislocalization problems associated with over-expression. Our results confirm that the majority of the mitotic Golgi is in a dispersed vesicular pool independent of the ER. In addition, the dispersed vesicles can be induced by perturbation of the mitotic spindle to rapidly coalesce with the larger structures to form membrane aggregates that are clearly distinct from the ER. These observations suggest that Golgi inheritance might be achieved by Golgi vesiculation followed by motility mediated dispersal of the vesiculated membranes.

Results

Separation of mitotic Golgi vesicles and ER by velocity gradient sedimentation

As expected, based on our previous work (24), the Golgi in nocodazole-arrested HeLa cells fractionated as membranes of two size classes after velocity gradient analysis (Figure 1A). As marked by the presence of two Golgi integral membrane proteins, giantin (28) and GPP130 (29), approximately 75% of the Golgi was recovered in a vesicle peak. Based on our previous determination of their S-value (115S), uniform migration over time, and measured diameter (60nm), the size of these vesicles is mostly homogenous and is similar to the size of COPI vesicles (24). In contrast to the Golgi, the mitotic ER (as marked by the presence of the ER integral membrane protein p63 (30,31), was recovered only as large membranes and not detected in the Golgi vesicle peak (Figure 1A).

Because microtubule disruption by nocodazole causes the Golgi complex to fragment and redistribute to peripheral sites in interphase cells, and because the formation of scattered Golgi stacks is caused, at least in part, by the cycling of Golgi enzymes through the ER and reemergence at ER exit sites (15–17), we tested whether nocodazole arrest might influence the fractionation behavior of the mitotic Golgi and ER (26). Therefore we performed velocity gradient analysis on otherwise untreated cells shaken from plates 9h after release from an S-phase block (as described in Methods). These cells exhibited a mitotic index of greater than 95% and, as judged by Hoechst 33258 staining of their condensed chromosomes, the majority were metaphase or anaphase. The fractionation profile observed for the same Golgi and ER markers in these cells was strikingly similar to that of the nocodazole-arrested cells (Figure 1B). Approximately 75% of the mitotic Golgi was recovered in small vesicles that lacked detectable ER.

We next attempted to exclude the formal possibility that the mitotic Golgi we recovered as vesicles was actually present in the ER at the time of our cell collection, but that the homogenization procedure caused preferential vesiculation of membranes containing Golgi markers (32). This explanation assumes that Golgi proteins partition into subdomains of the

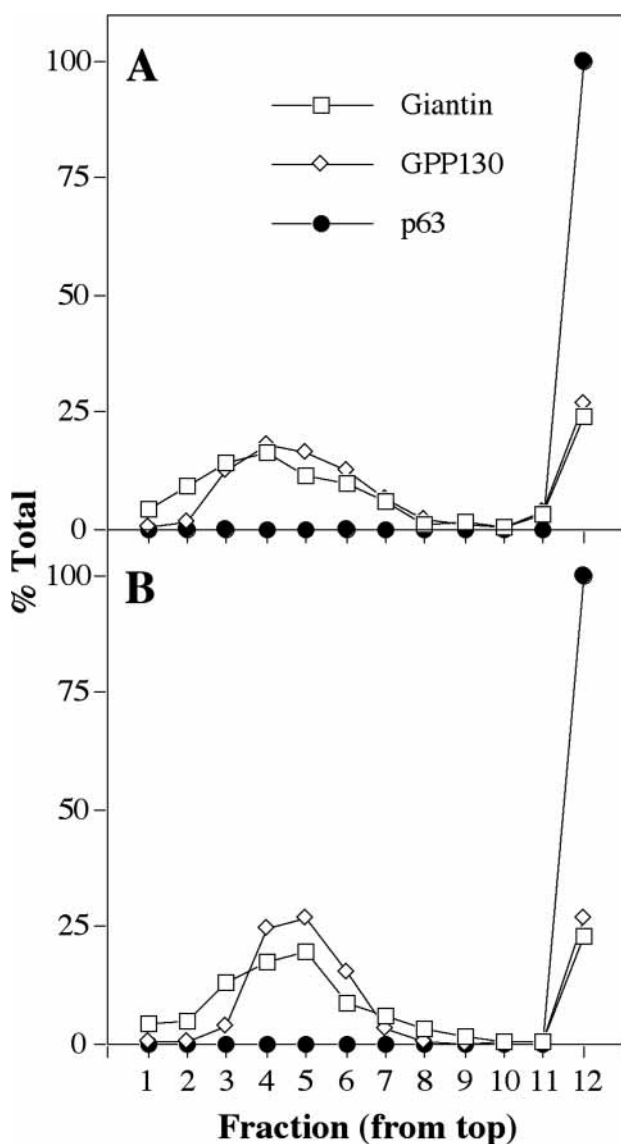


Figure 1: Separation of ER and mitotic Golgi vesicles. Mitotic HeLa cells, either nocodazole-arrested (A) or synchronized by the double-thymidine procedure (B) were collected by shake-off, mechanically homogenized and the resulting postnuclear supernatants were fractionated on a 5–25% glycerol velocity gradient. The relative distributions of giantin, GPP130, and p63 were determined by immunoblotting. The plotted values are averages from two separate experiments.

ER that lack the ER markers we previously analyzed: p63, glucose-6-phosphatase and calnexin (24). Therefore we compared the fractionation behavior of giantin, GPP130 and p63 on velocity gradients after different types of cell disruption. Our standard procedure had been passage of mitotic cells through a 25-gauge needle. To release the mitotic Golgi vesicles without mechanical disruption we treated nocodazole-arrested mitotic cells with digitonin, a detergent that selectively binds to cholesterol, leading to plasma membrane permeabilization (33). After a 20-min membrane release in-

cubation at 4°C, the released membranes were separated from the permeabilized cells by low-speed centrifugation. Approximately 40% of each Golgi marker was released from the cells, while less than 10% of the ER marker was released (not shown). Analysis of the released membranes on velocity gradients indicated that Golgi vesicles with the same sedimentation behavior as those present after mechanical disruption were abundantly present and lacked detectable ER (Figure 2A).

We also permeabilized cells by a freeze–thaw technique that was previously used to collect Golgi-derived vesicles (34). Similar to the results for digitonin permeabilization, approximately 40% of the Golgi was released from mitotic cells after freeze–thaw, while less than 10% of the ER was released (not shown). The fractionation profile of the released membranes (Figure 2B) was identical to digitonin-permeabilized cells (Figure 2A) and to membranes prepared under our standard homogenization conditions (Figure 1). We also obtained similar results using the freeze–thaw technique to analyze nonarrested synchronized cells shaken from plates at mitosis. In this case the ER membranes released from the cells, if any, were not sufficient to detect, while the released Golgi membranes migrated in the vesicle position of the gradient (Figure 2C). Therefore, we have obtained no evidence that nocodazole-arrest or mechanical homogenization causes mitotic Golgi vesicle formation by some aberrant process. Rather, a straightforward analysis of mitotic cells by subcellular fractionation demonstrates that the majority of the Golgi is present as small COPI-sized vesicles that are independent of the ER.

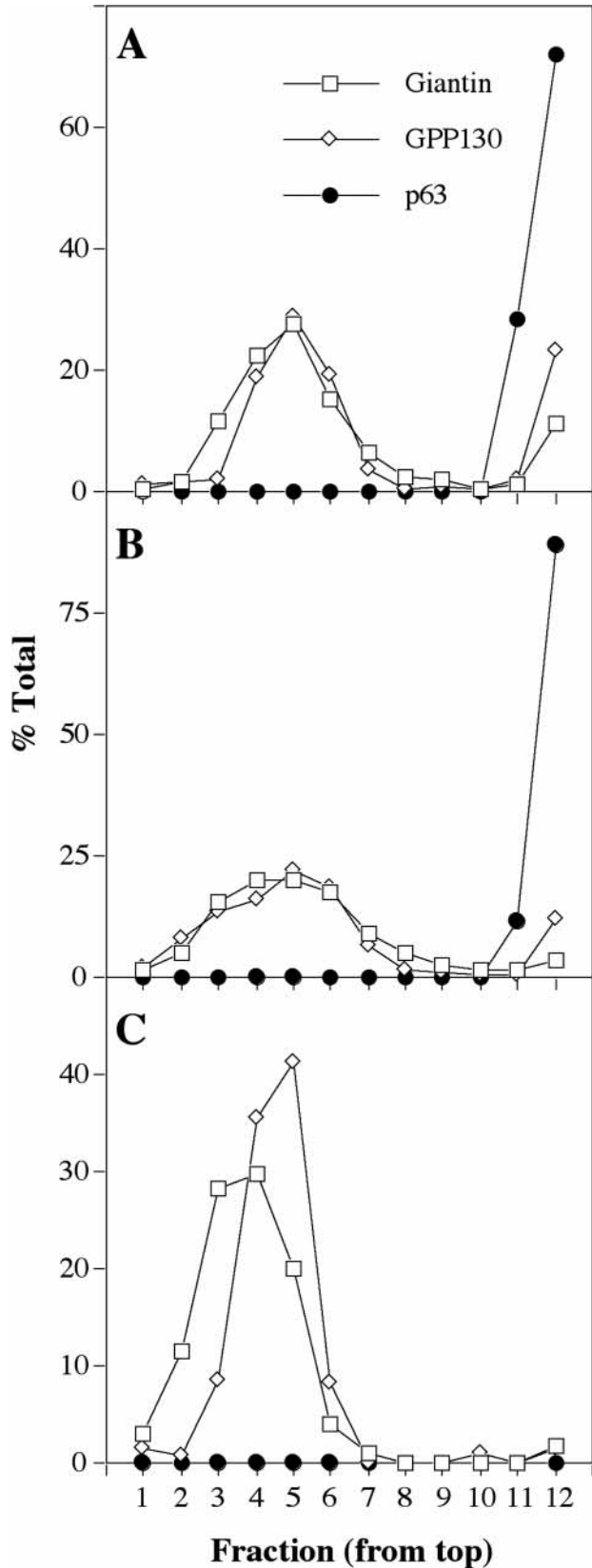
Noncoincidence of mitotic Golgi and ER by immunofluorescence with 3D reconstruction

The analysis above confirms that the ER and Golgi are not fused in mitotic HeLa cells. To extend this finding by analysis of intact cells, and to address whether the mitotic Golgi vesicles are dispersed throughout the cell or present as approximately 130 discrete objects, previously identified as vesicle clusters (2), we carried out a microscopic analysis of fixed metaphase cells. The primary goal was to carry out a 3D analysis, because previous analyses relied on 2D projections of 3D data. Such projections, particularly when using the maximum value of all aligned Z-axis pixel values instead of their sum, severely under-represent dispersed fluorescence (35). Thus, it was possible that the previously identified clusters actually represent only a small portion of the mitotic Golgi. To this end we carried out our analysis by collecting a stack of images by deconvolution microscopy. The deconvolved images were analyzed as single sections or in three dimensions. A secondary goal was to reduce experimental bias and account for possible variation between cells. Thus, a statistical analysis was carried out on results from multiple cells for each condition and each cell was chosen solely on the basis of its DNA staining. Finally, we sought to use endogenous integral membrane protein markers for the Golgi and ER to avoid the various problems associated with transgene expression.

The deconvolved images demonstrated an obvious lack of coincidence between Golgi and ER staining, as previously noted in our analysis using conventional fluorescence microscopy (24). The Golgi marker giantin was in membranes distributed throughout the cell but excluded from a narrow area corresponding to region containing condensed chromatin (Figure 3A). In contrast, the ER marker p63 appeared to be excluded from a larger region containing the mitotic spindle (Figure 3B). The spindle location was determined by DNA staining of the metaphase plate (Figure 3C), as well as by microtubule staining (see below). To analyze this discrepancy quantitatively for a single Z-axis section through the spindle of each cell, we compared the Golgi and ER fluorescence intensity in the zone of apparent ER exclusion vs. that in an identical sized area outside this region. The ER staining density in the excluded zone was only $20 \pm 7\%$ ($n = 10$) of that in the outer region. In contrast, the Golgi staining density in the same area was $100 \pm 20\%$ ($n = 10$) of that in the outer region. As a control for these experiments, we also compared the giantin and p63 staining patterns in cells that, prior to their entry into mitosis, had been treated with brefeldin A. Brefeldin A causes fusion of ER and Golgi in interphase cells (36), and treatment prior to M-phase entry results in an artificially induced state of ER/Golgi fusion in mitotic cells (24). As expected, the ER and Golgi staining patterns were coincident in these cells and the Golgi marker giantin was now largely excluded from the region occupied by the mitotic spindle (Figure 3D–F). This control indicated that exclusion from the spindle region is a property of the ER that is not shared by the Golgi and not the result of an anomaly of staining.

Another significant difference between the Golgi and ER staining patterns was the presence of relatively large objects in the Golgi pattern (Figure 3A). Compared to the abundant hazy staining that surrounded these objects, the larger objects were clearly resolvable and were absent in the ER pattern (Figure 3B). As expected for Golgi membranes independent of ER membranes, the larger Golgi objects were occasionally detected in the ER-free spindle region and they were not observed in control cells that, prior to their entry into mitosis, had been treated with brefeldin A (Figure 3D). The presence of both resolvable and nonresolvable object staining in the Golgi pattern was intriguing. The fractionation data presented above indicated that mitotic Golgi membranes consisted of both an abundant vesicle population and larger-sized membranes. Because the

Figure 2: Separation of ER and mitotic Golgi vesicles released from permeabilized cells. Mitotic HeLa cells, either nocodazole arrested (A and B) or synchronized by the double-thymidine procedure (C) were collected by shake-off. The cells were then either digitonin permeabilized (A) or freeze/thaw permeabilized (B and C) and the released membranes were fractionated on 5–25% glycerol velocity gradients. The relative distributions of giantin, GPP130, and p63 were determined by immunoblotting. The plotted values are averages from two separate experiments.



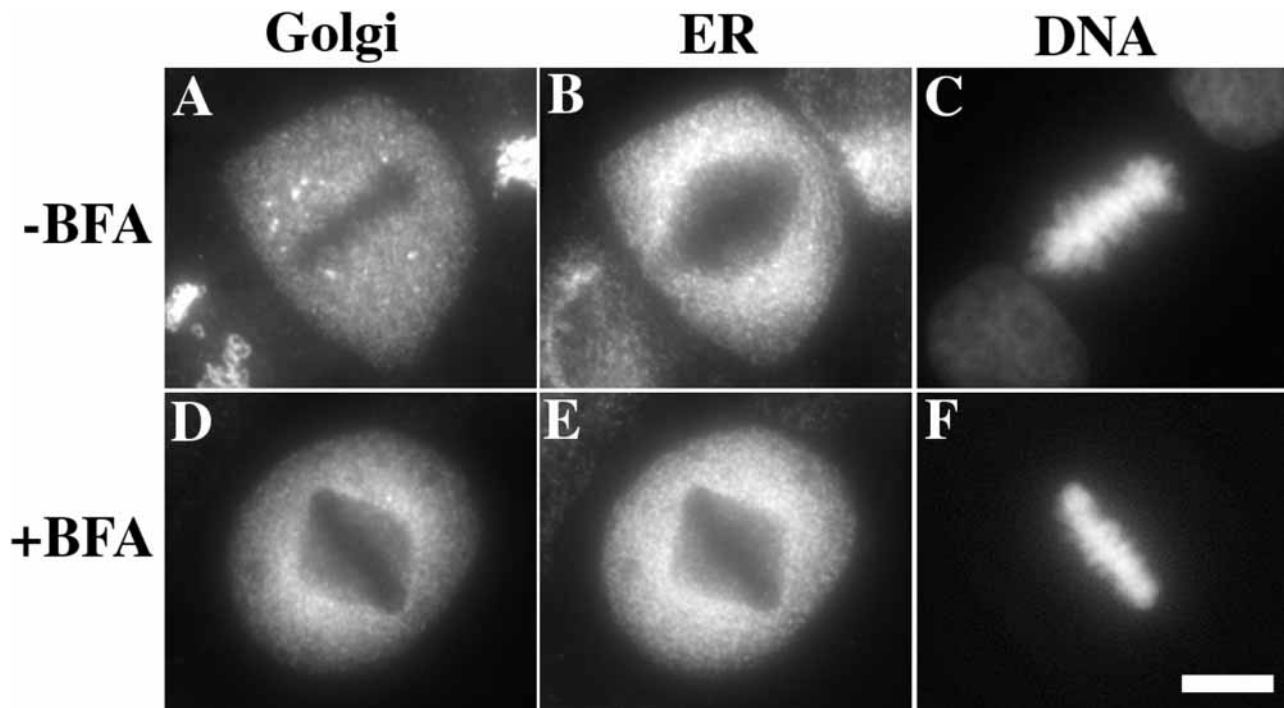


Figure 3: Absence of ER, but not mitotic Golgi, from the spindle area. HeLa cells were incubated in the absence (A–C) or presence (D–F) of 10 μ g/ml brefeldin A (BFA) at 37°C for 3 h. Cells were fixed and triply stained for the Golgi marker giantin (A and D), the ER marker p63 (B and E), and the DNA stain Hoechst 33258 (C and F). The images shown are 2D projections from the deconvolved 3D data set using summation of pixel values in each plane. Bar = 10 μ m.

small vesicles have a diameter less than the limit of resolution by light microscopy, it was likely that the nonresolvable staining corresponded to dispersed mitotic Golgi vesicles. Note that the nonresolvable, or hazy, fluorescence was significantly above background (see below). Similarly, the larger objects in both the fractionation experiments and in the fluorescent staining pattern probably represent, at least in part, mitotic Golgi in the form of vesicle clusters and/or cisternal remnants (2,23,25).

To provide a quantitative assessment of the distribution of Golgi between the larger resolvable objects and the smaller nonresolvable objects in intact metaphase cells, the resolvable objects were identified in three dimensions and the fraction of total fluorescence comprised by these objects was determined. On a per cell basis, there were 170 ± 50 ($n = 8$) objects and these were on average 480 nm in diameter, but the objects accounted for only $2.2 \pm 0.8\%$ ($n = 8$) of the total fluorescence signal (see also Table 1). Thus, although the object number and average size closely match the values previously reported for vesicle clusters (2,25,37), our analysis indicates that these clusters only represent a small fraction of the mitotic Golgi.

This analysis involved determination of two critical values: background and threshold. The background value was determined from analysis of metaphase cells stained with secondary antibody only (see Methods) and was then subtracted

from each voxel in the 3D data set. Threshold was determined manually (see Methods) and groups of voxels were then identified as objects if their intensity was above the threshold value. To test the sensitivity of object discrimination to changes in threshold value, we calculated object number for each cell in the data set using threshold values above and below the manually chosen value. Consistent with the expectation that an optimum threshold value will be the lowest value at which object number is relatively constant, we observed a relatively constant number of objects at values just above the assigned value and a rapid increase in object number just below (Figure 4A). At values below an optimum threshold value it is expected that minor fluctuations in fluorescence will be counted as objects and result in the inclusion of numerous artifactual objects. For the purpose of representation, an original gray-scale image (Figure 4B) and its thresholded counterpart (Figure 4C) are shown as summed 2D projections. Also shown as a summed 2D projection, is the distribution of the subthreshold fluorescence that corresponds to the major fraction of the mitotic Golgi (Figure 4D). The potential for under-representation of dispersed staining is illustrated for the same cell in a maximum value projection (Figure 4E) and in an image of a single optical section (Figure 4F). Abundant dispersed staining was also observed in metaphase NRK cells, and it was also observed with two other types of microscopy that eliminate out-of-focus fluorescence: confocal and grating-imager microscopy. Together with the velocity gradient analysis above,

Table 1: Analysis of metaphase Golgi object number, size, and percent of total

Treatment	Number of objects (per cell)	Average object diameter (nm)	% Fluorescence in objects
37°C	170 ± 50	480 ± 30	2.2 ± 0.8
15°C	200 ± 80	720 ± 60	9 ± 2
Nocodazole	200 ± 70	610 ± 68	6 ± 4
DOG azide	140 ± 70	680 ± 90	8 ± 4

HeLa cells were incubated at 37°C, 15°C for 30 min, 37°C for 30 min with 10 µg/ml nocodazole, or 37°C for 30 min with DOG azide. After fixation and staining using the Golgi marker giantin, optical sections were acquired by deconvolution and the fluorescence distribution in objects was analyzed. Average value with standard deviation is presented.

these experiments suggest that the major partitioning unit of the Golgi in these cells is uniformly dispersed vesicles.

Surprisingly, in metaphase cells that were briefly shifted to reduced temperature, the percentage of Golgi fluorescence present in resolvable objects increased at the expense of the fluorescence in nonresolvable objects. For example, in contrast to its normal pattern (Figure 3A), the Golgi pattern after a 30-min 15°C incubation was markedly more punctate with reduced haze (Figure 5A). The ER pattern in the same cells did not show this change (Figure 5B). Again as a control, we used brefeldin A treatment prior to M-phase entry to cause fusion of the ER and Golgi. In this case the Golgi pattern was coincident with the ER, and similar to the ER pattern, it did not become more punctate upon reduced temperature incubation (Figure 5D). The conversion of the Golgi pattern was rapid, exhibiting an apparent $t_{1/2}$ of 5 min (Figure 6A). This argues against any significant change in cell cycle state of the cells being responsible for the altered Golgi pattern. The redistribution of Golgi upon temperature shift was also analyzed quantitatively in 3D. Although the number of objects per cell was not significantly different, the fluorescence in resolvable objects was increased 4-fold and the average object size increased from 480 nm to 720 nm (Table 1). Indeed, the frequency distribution of object sizes showed a marked shift from size classes less than 400 nm to sizes above this value (Figure 6B). Because the object number was not significantly altered by temperature shift, this analysis indicated that fluorescence attributed to dispersed vesicles redistributed into mostly pre-existing objects that, as a consequence, became larger in size. The observation that the ER in the same cells did not undergo this redistribution provides further evidence that the abundant dispersed fluorescence represents small vesicles that are independent of the ER.

Inspection of the ER staining pattern in cells treated at 15°C revealed an apparent reduction of its exclusion from the spindle region (Figure 5B). Together with the known destabilizing effect of reduced temperature on microtubules, this suggested that an alteration in spindle structure might be related to the change in mitotic Golgi distribution. Therefore we stained microtubules in metaphase cells after shift to 15°C. As expected, untreated metaphase cells exhibited a normal dispersed Golgi pattern (Figure 7A) and a typical spindle staining pattern (Figure 7B). In contrast, the shifted

cells exhibited a largely punctate Golgi pattern and a dramatically reduced spindle pattern (Figure 7E). Thus, loss of spindle structure correlated with the redistribution of mitotic Golgi and is likely to account for the movement of the ER into the spindle region. If microtubule integrity and/or microtubule-based motor function is required to maintain the uniform dispersal of mitotic Golgi vesicles, then treatment of cells at 37°C with agents that disrupt these functions should cause Golgi clustering. Indeed, brief nocodazole treatment led to depolymerization of spindle microtubules (Figure 7H) and to increased apparent vesicle clustering (Figure 7G). Increased apparent vesicle clustering was also observed after brief treatment with deoxyglucose/azide to block ATP-dependent cellular functions (Figure 7J). As expected, this treatment also disrupted spindle structure (Figure 7K). For each of the treatments, changes in the fraction of Golgi in resolvable objects, as well as changes in object number and size, were determined. Each treatment caused a redistribution that was similar in extent to that caused by 15°C (Table 1). In summary, the Golgi in metaphase HeLa cells is largely present as uniformly dispersed vesicles that have a capacity to undergo ATP-independent association with, at least in part, pre-existing larger Golgi elements (or remnants after breakdown). This capacity for association appears to be negatively influenced by a mechanism that requires microtubule integrity.

Discussion

The importance of knowing the state of the disassembled Golgi at M-phase is two-fold. It elucidates the inheritance strategy that evolved to achieve accurate Golgi partitioning, and it suggests the underlying mechanism. Our results indicate that the major breakdown product is dispersed vesicles that are independent of the ER. In addition, these vesicles appear to be in a microtubule-dependent equilibrium with larger structures. Presumably, the larger structures represent vesicle clusters, as their size and number matched previous reports (2,23,25). Our results suggest that two steps – vesiculation and dispersal – comprise the inheritance strategy that evolved for the mammalian Golgi. In terms of the underlying mechanism, vesiculation is best accounted for by inhibition of docking and/or fusion, and dispersal is best accounted for by a combination of microtubule-motor-mediated membrane dispersal and Brownian motion.

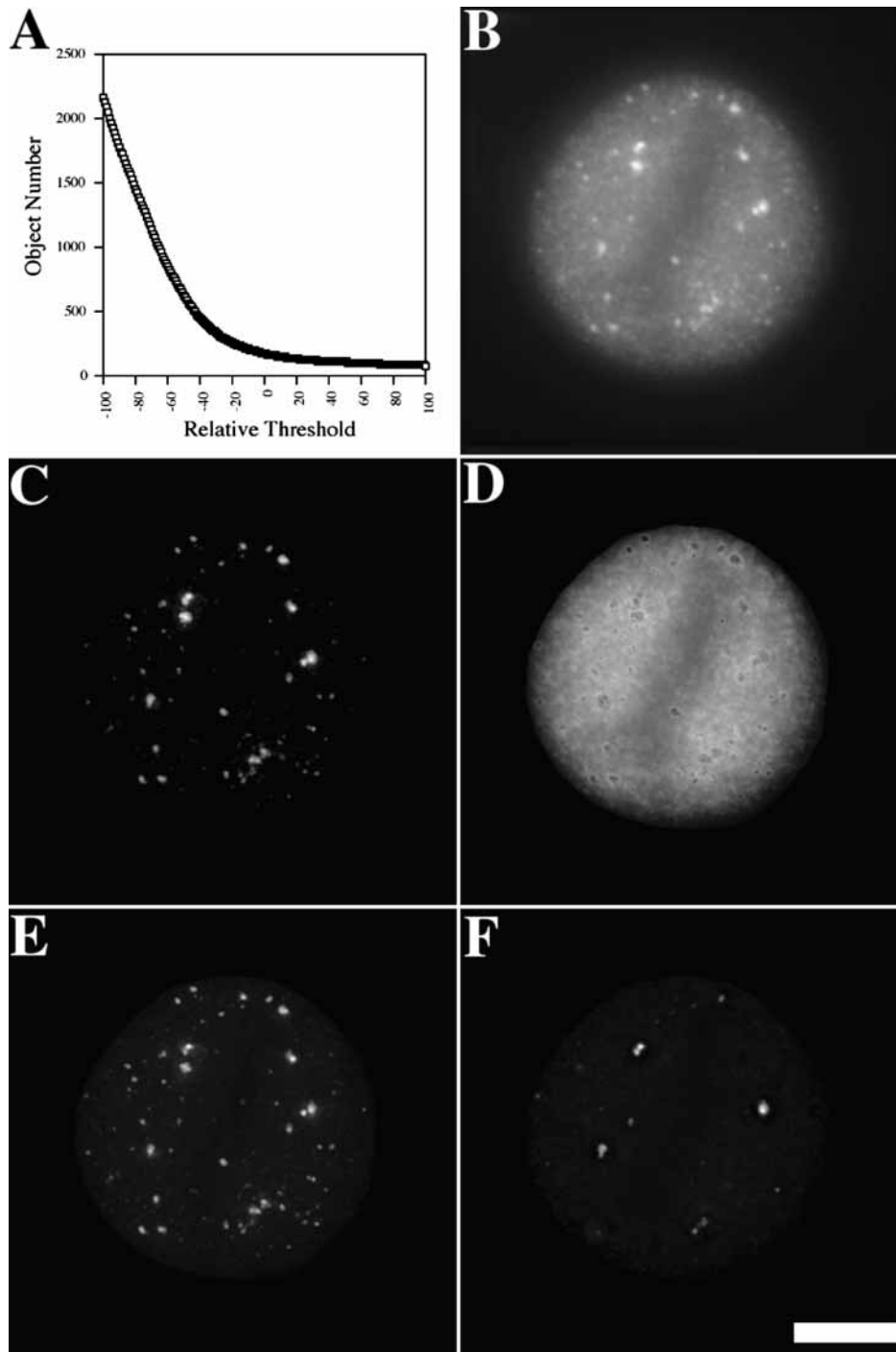


Figure 4: Analysis of 37°C metaphase HeLa cells. The average number of objects per cell, determined for 8 metaphase cells at various threshold values, is plotted relative to the manually chosen threshold value for each cell (A). Three summed 2D projections are shown for a representative metaphase cell. The first is the gray-scale image prior to background subtraction (B). The second is the image after masking, background subtraction, and thresholding (C). The third represents only that fluorescence removed by the thresholding step (D). Also shown for the same cell is a maximum value projection (E) and a single optical section (F). For viewing, the images were scaled using values of 11 977, 5573, 5573, 1700, and 1423, respectively. Bar = 10 μ m.

The evidence for M-phase Golgi vesiculation is compelling. A mostly dispersed staining pattern for Golgi markers is observed in metaphase cells. As would be expected for dispersed small vesicles, this pattern is comprised of fluorescence in nonresolvable objects that are not coincident with the ER. Further, fractionation of M-phase cells, either arrested or not, and either with or without mechanical homogenization, yields a vesicle peak containing the majority of the mi-

totic Golgi. Golgi vesicles in M-phase cells have been documented by EM (22,23) and Golgi vesicles are also the major breakdown product of isolated Golgi incubated with mitotic cytosol (13). The suggestion that accumulation of these vesicles is the consequence of inhibition of docking and/or fusion fits well with the available evidence. As mentioned above, mitotic phosphorylation of GM130 significantly reduces its affinity for p115 (12) and this could prevent docking

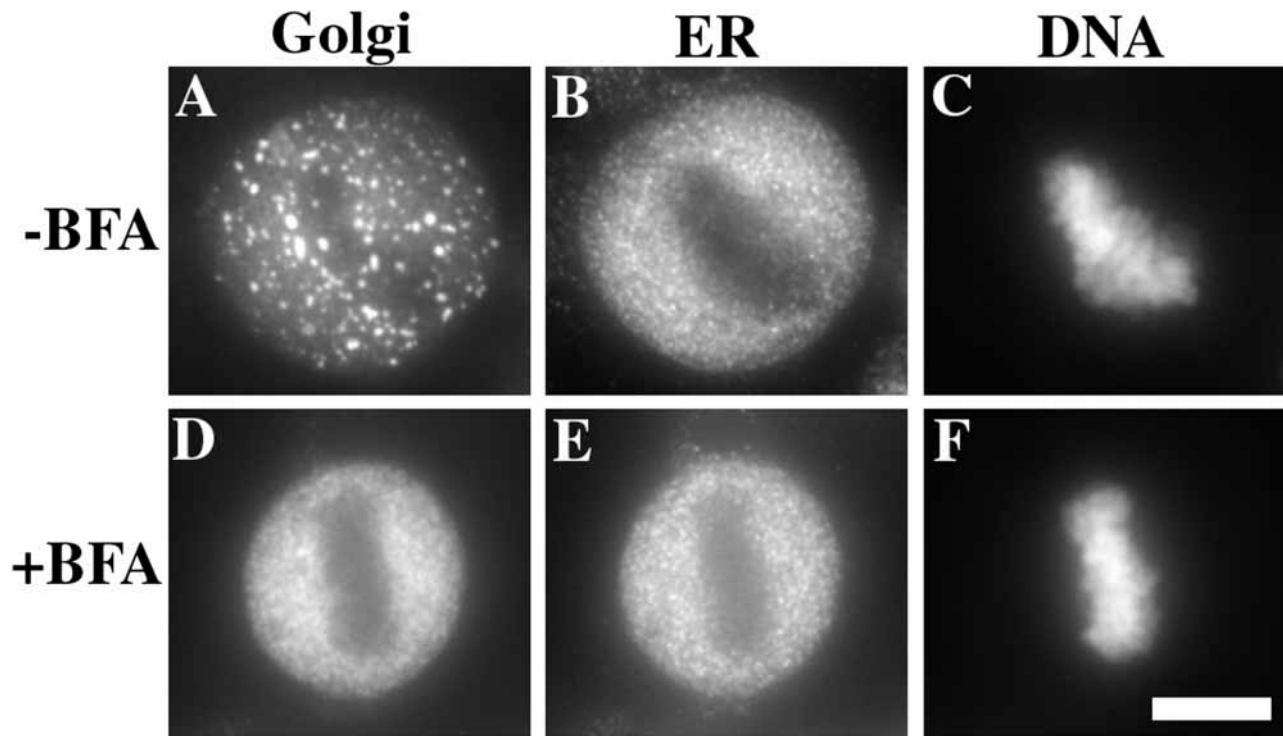


Figure 5: Induction of mitotic Golgi clustering by incubation at 15°C. HeLa cells were incubated in the absence (A–C) or presence (D–F) of 10 μ g/ml brefeldin A (BFA) at 37°C for 3 h. Cells were fixed and triply stained for giantin (A and D), p63 (B and E) and Hoechst 33258 (C and F). The images are summed 2D projections. Bar = 10 μ m.

(7) and subsequent fusion of COPI retrieval vesicles containing Golgi residents. The effectiveness of this block in transforming the Golgi into vesicles would also be increased by a simultaneous block in ER-to-Golgi transport (10).

That the vesicles are dispersed is clear from their staining pattern, and this would account for accurate Golgi inheritance in the absence of an active mechanism. Nevertheless, spindle microtubules, and presumably microtubule-based vesicle motor activity, appear to contribute to the generation of the dispersed vesicle state. During *in vitro* mitotic Golgi breakdown a small fraction of the Golgi remains as larger structures, the so-called Golgi remnants. We suggest that weak interactions between mitotic Golgi remnants and vesicles generate the vesicle clusters visualized by EM and that microtubule-based motor activity plays a role in breaking apart these interactions to distribute the vesicles. This follows from the observation that treatments of metaphase cells that perturb the integrity of the spindle by disrupting microtubules causes a rapid increase in the amount of Golgi that is present in larger resolvable objects. This increase came at the expense of the dispersed fluorescence, and resulted in an increased average size but not increased object number.

This observation helps explain the controversy surrounding reports concluding that the mitotic Golgi is present as a discrete number of clusters (2,20). If clusters are in equilibrium with dispersed vesicles, then different cell types and culture

conditions could contribute to different states of the mitotic Golgi. Nevertheless, our quantitative analysis indicated that, at least for HeLa cells, the representation of the Golgi in larger structures was about 2%. This fits remarkably well with an immuno-EM-based estimate in which mitotic Golgi clusters accounted for < 5% of interphase Golgi volume (37). Previous over-representations of clusters were probably due to analysis of maximum value 2D projections and insufficient accounting for fluorescence loss due to thresholding (2,20). At best, any quantitative analysis of fluorescent objects is an approximation. In our case, even though 3D analysis reduces the error, the amount of fluorescence attributed to objects underestimates the actual value due to inherent limits of thresholding and light microscopy. We verified that our threshold values approximated the lowest value yielding a stable number of objects. Although this attempts to maximally represent the fluorescence in these objects, many were probably surrounded by subthreshold voxels that ideally should be included. Of course, if the threshold were lowered to include these voxels, artifactual objects would become above threshold throughout the image. In any event, because these surrounding values are low relative to the above-threshold values, and because the amount of total fluorescence in objects was low, we can conclude that most of the mitotic Golgi is present in small dispersed vesicles.

This analysis, as well as previous reports (2,10,20,24), argue against Golgi fusion with the ER (21), contributing significant-

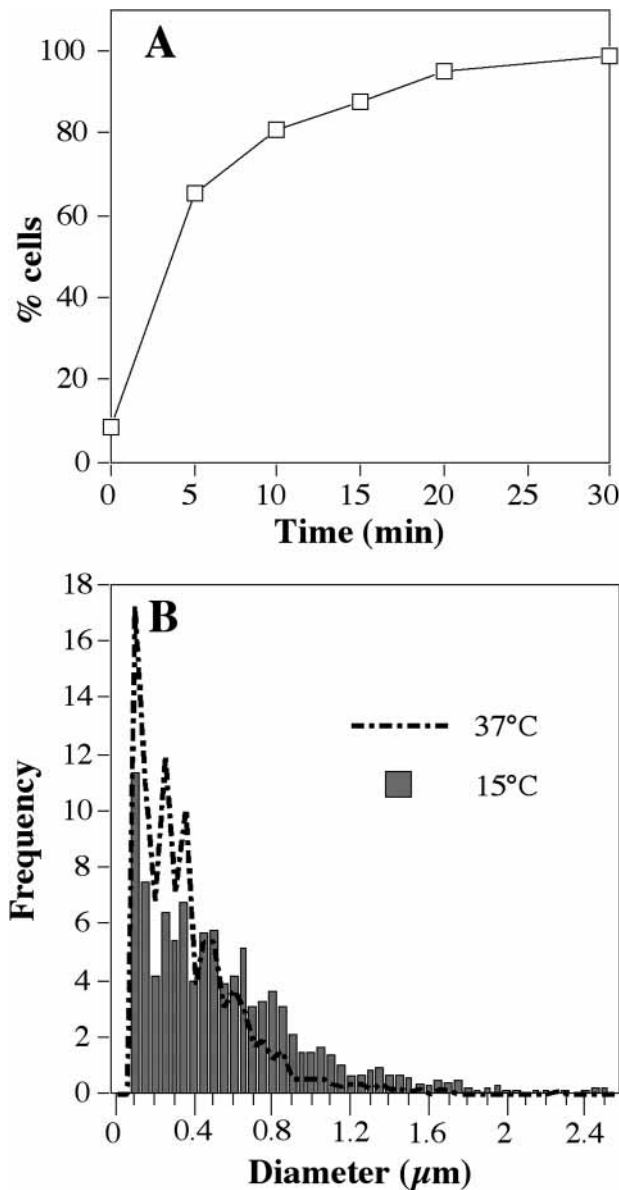


Figure 6: Rate and size distribution of mitotic Golgi cluster formation. HeLa cells were incubated at 15°C for various times then immediately fixed and triply stained for the Golgi markers giantin and GPP130 and the DNA stain Hoechst 33258. For each time point, 30 metaphase cells were examined at a mid-cell focal plane and those with >20 large objects (>0.2 μm) were scored as clustered. The percentage of clustered cells at each time point is plotted (A). The values are averages of two independent experiments. Also shown is the frequency distribution of object size in the 3D data sets for metaphase cells that were either not shifted (37°C) or shifted to 15°C for 30 min prior to fixation (B).

ly to the overall process of Golgi partitioning. Upon fractionation, the Golgi-derived vesicles lacked ER markers. And, in intact cells, they exhibited two attributes that were distinct from the ER: penetration of the spindle region and redistribution into larger structures upon spindle disruption. Nevertheless, increasing evidence suggests both constitutive and

regulated recycling of Golgi proteins through the ER (16,38,39). Also, all newly synthesized integral Golgi proteins are present in the ER transiently. Thus, it seems reasonable that during mitosis some fraction of Golgi proteins are in the ER to begin with and that another fraction redistributes to the ER due to on-going Golgi-to-ER recycling. This would account for detection of Golgi proteins in the mitotic ER by immuno-EM (21,40). But, the rates of new synthesis and recycling are relatively slow, limiting the extent to which Golgi proteins are ER-localized at metaphase. For the Golgi markers we tested, which include enzymes and putative structural proteins, representing both *cis* and *trans* cisternae localizations, the upper limit for redistribution to the ER is 25%, and it is likely to be significantly less (24). Previous work may have overestimated the extent of Golgi in the ER due to the use of tagged overexpressed proteins that appeared to be, at least partially, mislocalized (21). The experiments reported here do not rule out the possibility of synchronous or asynchronous passage of the entire Golgi into and back out of the ER prior to metaphase. Nevertheless, among other results, the aforementioned M-phase block of ER export makes this possibility unlikely (10).

The presence of numerous small Golgi vesicles is consistent with the idea that Golgi inheritance is passive. However, uniform dispersal of these vesicles must be maintained prior to cell cleavage. Although spindle microtubules are not required for Golgi vesicle dispersal, our finding that they somehow mediate cluster disruption, together with observations of mitotic Golgi movement on spindle microtubules (20), suggests that accurate Golgi inheritance is not entirely passive. Of course, a specific inhibitor of the putative microtubule-based motor responsible for cluster disruption is needed to determine the significance of this activity. In any event, our experiments indicate that if there is an active mechanism, it mediates membrane dispersal, not a directed membrane movement akin to spindle-mediated chromosome inheritance. This can explain why, in contrast to chromosome partitioning, Golgi partitioning is expected to be proportional to the size of the daughter cells and therefore unequal during asymmetric division.

Materials and Methods

Cell culture

HeLa cells were grown in minimal essential medium (Life Technologies, Grand Island, NY, USA) supplemented with 10% fetal bovine serum and 100 IU/ml penicillin-streptomycin (Life Technologies). Where indicated, the growth medium was supplemented with 2mM thymidine (Calbiochem-Novachem Corp., La Jolla, CA, USA), 0.5 $\mu\text{g/ml}$ nocodazole (Sigma, St. Louis, MO, USA), 10 $\mu\text{g/ml}$ brefeldin A (Sigma), 50mM deoxyglucose (Sigma), or 0.02% sodium azide (Sigma). For fractionation experiments, mitotic cells were isolated by shake-off from subconfluent cultures that were either synchronized or arrested. M-phase synchronization was achieved as follows: 24h incubation with thymidine, three washes and 16h incubation in thymidine-free medium, 14h incubation with thymidine, three washes and 9h incubation in thymidine-free medium (41). M-phase arrest was achieved by an 18–20h incubation with nocodazole (42). To

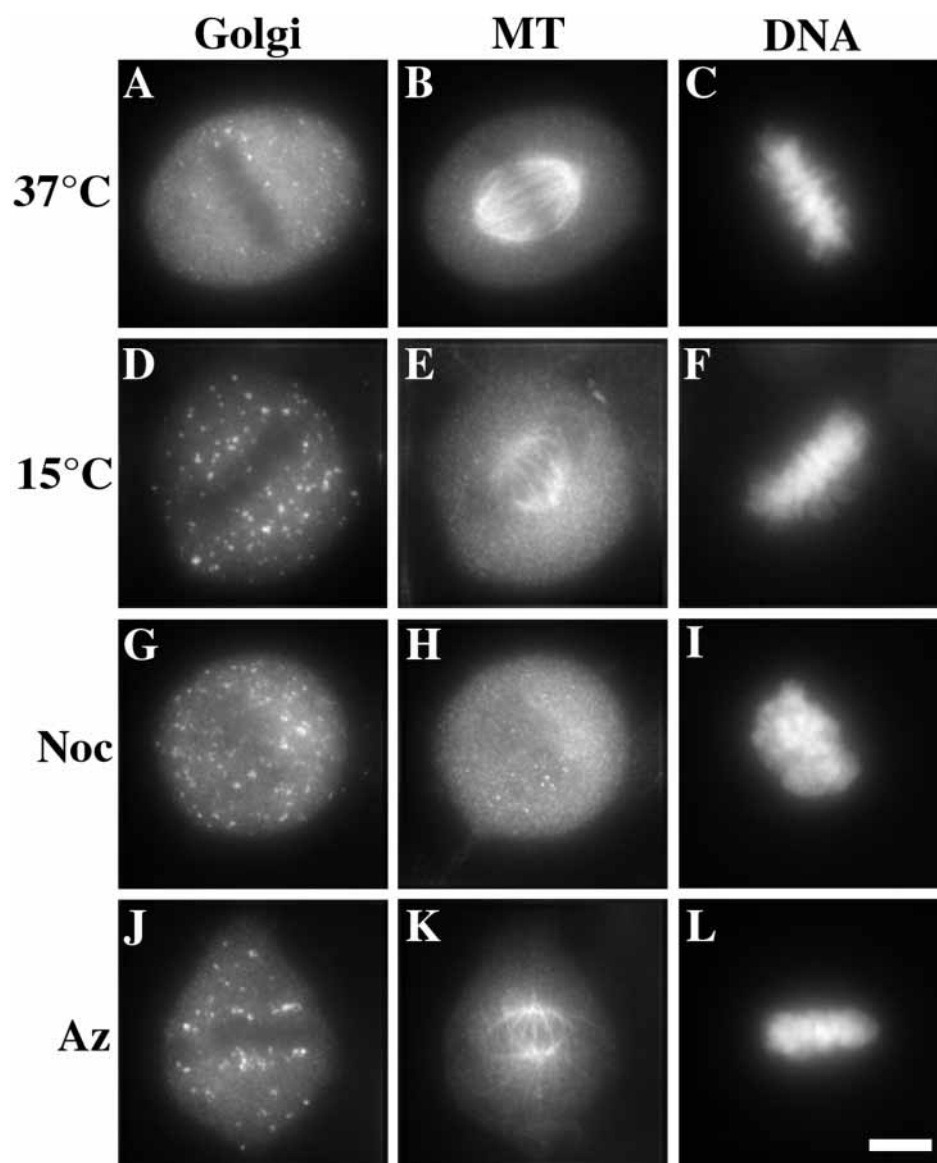


Figure 7: Spindle destabilization correlates with mitotic Golgi cluster formation. HeLa cells were incubated at 37°C (A–C), 15°C for 30 min (D–F), 37°C for 30 min with 10 µg/ml nocodazole (G–I), or 37°C for 30 min with DOG azide (J–L). After each treatment, cells were fixed and triply stained for the Golgi marker GPP130 (A, D, G, and J), the microtubule marker beta-tubulin (B, E, H, and K), and the DNA marker Hoechst 33258 (C, F, I, and L). The images are summed 2D projections. Bar = 10 µm.

determine mitotic index, a sample of cells was resuspended in 3% paraformaldehyde, 0.2% Triton X-100, 2 µg/ml Hoechst 33258, incubated on ice for 10 min and examined by fluorescence microscopy as described (29). For immunofluorescence microscopy of metaphase cells, HeLa cells were grown on 22-mm glass coverslips and then treated as indicated. Transfer to 15°C was carried out by exchange of the media with prechilled growth medium containing 10 mM HEPES, pH 7.4 and incubation in a 15°C water bath.

Velocity gradient fractionation

All steps were carried out at 4°C in the presence of protease inhibitors (1 mM phenylmethylsulfonyl fluoride, 10 µg/ml leupeptin, and 10 µg/ml pepstatin A) unless otherwise indicated. Intracellular membranes were released from washed mitotic cells by mechanical homogenization, digitonin permeabilization, or freeze–thaw permeabilization and collected as a supernatant after centrifugation at 1000 × g for 2 min. For mechanical homogenization, cells were passed through a 25-g needle in homogenization buffer (50 mM NaCl, 10 mM triethylamine, pH 7.4, 1 mM EDTA) as described (24). For digitonin permeabilization, cells were rotated in homogen-

ization buffer containing 0.003% digitonin (Sigma) for 20 min at 4°C (6). For freeze–thaw permeabilization, cells were resuspended in 4 cell volumes of homogenization buffer, snap frozen in liquid nitrogen, stored at –80°C until needed, and thawed in a water bath at room temperature (34). Supernatants (0.4 ml) were layered on linear 5 ml 5–25% glycerol gradients containing a 0.5-ml 80% sucrose cushion and centrifuged at 150 000 × g for 30 min in a SW50.1 rotor (Beckman, Fullerton, CA, USA), and 0.4 ml fractions were collected from the top (24). After 3.75-fold dilution, proteins in each fraction were precipitated with trichloroacetic acid as described (43), separated by SDS-PAGE and immunoblotted with anti-giantin (1 : 5000) (44), anti-GPP130 (1 : 100) (29), and anti-p63 (1 : 10 000) (45), as previously described (28). Detection was by enhanced chemiluminescence (Pierce, Rockford, IL, USA) with quantification using NIH Image 1.62 software.

Immunofluorescence microscopy and analysis

Cells were fixed in 3% paraformaldehyde and processed exactly as described (24), using anti-p63 (1 : 100), anti-giantin (1 : 1000), anti-GPP130 (1 : 200), or anti-β-tubulin rabbit antibody (1 : 200, ICN Biomedicals, Inc.,

Irvine, CA, USA). Coverslips were attached to glass slides over mounting medium (0.1 mg/ml phenylenediamine in glycerol) containing 2 µg/ml Hoechst 33258. Except where indicated, microscopy was performed using a Deltavision system (Applied Precision Inc., Issaquah, WA, USA) equipped with a 60 × 1.4 na oil immersion objective yielding a pixel dimension of 0.1114 µm. Three-channel images were acquired at 0.3-µm steps through each metaphase cell and deconvolved using Softworx (Applied Precision Inc.). To determine the extent of exclusion from the spindle region, an optical section corresponding to the center of each cell (section 20 out of 40) was chosen. Background was subtracted using the most common extracellular pixel value and the amount of fluorescence in each channel in a fixed-size area both inside and outside the spindle region was obtained using NIH Image (v 1.62).

Quantification of the 3D data set was carried out using Matlab (Mathworks Inc., Natick, MA, USA). Total fluorescence was the sum of all fluorescence, after background subtraction, included in a mask manually created to separate each cell. The background value subtracted from each voxel was the most common voxel value outside the cell multiplied by a factor of 1.22. This factor was the average of a ratio (most common voxel value inside the cell/most common voxel value outside the cell) determined from the 3D data set of 4 metaphase cells that were stained with secondary antibody only. For object discrimination, threshold values were manually chosen for sections 10, 20, and 30 (out of 40) in each cell. Using the original gray-scale image as the standard, the attempt was made to maximize inclusion of discernible objects and minimize inclusion of nondiscernible objects. The average of the three values was then used as the threshold for that cell. Object finding was done on the thresholded image using 26-neighbor connectivity and the number of objects, the average object size, and the fraction of total fluorescence in objects were calculated. Object diameter was calculated from the maximum cross-sectional area in the XY plane for the object assuming a circular shape.

Quantification of mitotic Golgi cluster time courses was carried out using a 60 × 1.4 na oil immersion objective and a conventional fluorescence microscope. Metaphase cells containing greater than 20 structures in the cell center focal plane with an area greater than 0.2 µm² were counted as clustered (2). Thirty metaphase cells were counted for each time point.

Acknowledgments

We thank: Dr Z. Elazar for suggesting the digitonin release assay; Dr A. Csink and B. Sage for help with the Deltavision system; Dr F. Lanni for help with the grating imager and confocal analysis; Dr T. Lee, M. Puthenveedu, C. Bachert, and S. Puri for critical reading of the manuscript. This work was supported by NIH grant GM-56779-02 to A.D.L.

References

- Donaldson JG, Lippincott-Schwartz J. Sorting and signaling at the Golgi complex. *Cell* 2000;101:693–696.
- Shima DT, Haldar K, Pepperkok R, Watson R, Warren G. Partitioning of the Golgi apparatus during mitosis in living HeLa cells. *J Cell Biol* 1997;137:1211–1228.
- Pelham HR, Rothman JE. The debate about transport in the Golgi – two sides of the same coin? *Cell* 2000;102:713–719.
- Glick BS, Malhotra V. The curious status of the Golgi apparatus. *Cell* 1998;95:883–889.
- Burkhardt JK. The role of microtubule-based motor proteins in maintaining the structure and function of the Golgi complex. *Biochim Biophys Acta* 1998;1404:113–126.
- Acharya U, Mallabiabarrena A, Acharya JK, Malhotra V. Signaling via mitogen-activated protein kinase kinase (MEK1) is required for Golgi fragmentation during mitosis. *Cell* 1998;92:183–192.
- Lowe M, Rabouille C, Nakamura N, Watson R, Jackman M, Jamsa E, Rahman D, Pappin DJ, Warren G. Cdc2 kinase directly phosphorylates the cis-Golgi matrix protein GM130 and is required for Golgi fragmentation in mitosis. *Cell* 1998;94:783–793.
- Kano F, Takenaka K, Yamamoto A, Nagayama K, Nishida E, Murata M. MEK and Cdc2 kinase are sequentially required for Golgi disassembly in MDCK cells by the mitotic *Xenopus* extracts. *J Cell Biol* 2000;149:357–368.
- Dell KR, Turck CW, Vale RD. Mitotic phosphorylation of the dynein light intermediate chain is mediated by cdc2 kinase. *Traffic* 2000;1:38–44.
- Farmaki T, Ponnambalam S, Prescott AR, Clausen H, Tang BL, Hong W, Lucocq JM. Forward and retrograde trafficking in mitotic animal cells. ER–Golgi transport arrest restricts protein export from the ER into COPII-coated structures. *J Cell Sci* 1999;112:589–600.
- Prescott AR, Farmaki T, Thomson C, James J, Paccaud JP, Tang BL, Hong W, Quinn M, Ponnambalam S, Lucocq J. Evidence for prebud- ding arrest of ER export in animal cell mitosis and its role in generating Golgi partitioning intermediates. *Traffic* 2001;2:321–335.
- Nakamura N, Lowe M, Levine TP, Rabouille C, Warren G. The vesicle docking protein p115 binds GM130, a cis-Golgi matrix protein, in a mitotically regulated manner. *Cell* 1997;89:445–455.
- Misteli T, Warren G. COP-coated vesicles are involved in the mitotic fragmentation of Golgi stacks in a cell-free system. *J Cell Biol* 1994;125:269–282.
- Sonnichsen B, Lowe M, Levine T, Jamsa E, Dirac-Svejstrup B, Warren G. A role for giantin in docking COPI vesicles to Golgi membranes. *J Cell Biol* 1998;140:1013–1021.
- Cole NB, Sciaky N, Marotta A, Song J, Lippincott-Schwartz J. Golgi dispersal during microtubule disruption. regeneration of Golgi stacks at peripheral endoplasmic reticulum exit sites. *Mol Biol Cell* 1996;7:631–650.
- Storrie B, White J, Rottger S, Stelzer EH, Sukanuma T, Nilsson T. Recycling of Golgi-resident glycosyltransferases through the ER reveals a novel pathway and provides an explanation for nocodazole-induced Golgi scattering. *J Cell Biol* 1998;143:1505–1521.
- Drecktrah D, Brown WJ. Phospholipase A(2) antagonists inhibit nocodazole-induced Golgi ministack formation; evidence of an ER intermediate and constitutive cycling. *Mol Biol Cell* 1999;10:4021–4032.
- Hammond AT, Glick BS. Dynamics of transitional endoplasmic reticulum sites in vertebrate cells. *Mol Biol Cell* 2000;11:3013–3030.
- Girod A, Storrie B, Simpson JC, Johannes L, Goud B, Roberts LM, Lord JM, Nilsson T, Pepperkok R. Evidence for a COP-I-independent transport route from the Golgi complex to the endoplasmic reticulum. *Nat Cell Biol* 1999;1:423–430.
- Shima DT, Cabrera-Poch N, Pepperkok R, Warren G. An ordered inheritance strategy for the Golgi apparatus: visualization of mitotic disassembly reveals a role for the mitotic spindle. *J Cell Biol* 1998;141:955–966.
- Zaal KJ, Smith CL, Polishchuk RS, Altan N, Cole NB, Ellenberg J, Hirschberg K, Presley JF, Roberts TH, Siggia E, Phair RD, Lippincott-Schwartz J. Golgi membranes are absorbed into and reemerge from the ER during mitosis. *Cell* 1999;99:589–601.
- Lucocq JM, Berger EG, Warren G. Mitotic Golgi fragments in HeLa cells and their role in the reassembly pathway. *J Cell Biol* 1989;109:463–474.
- Misteli T, Warren G. Mitotic disassembly of the Golgi apparatus *in vivo*. *J Cell Sci* 1995;108:2715–2727.
- Jesch SA, Linstedt AD. The Golgi and endoplasmic reticulum remain independent during mitosis in HeLa cells. *Mol Biol Cell* 1998;9:623–635.
- Lucocq JM, Warren G. Fragmentation and partitioning of the Golgi

- apparatus during mitosis in HeLa cells. *EMBO J* 1987;6:3239–3246.
26. Roth MG. Inheriting the Golgi. *Cell* 1999;99:559–562.
 27. Colanzi A, Deerinck TJ, Ellisman MH, Malhotra V. A specific activation of the mitogen-activated protein kinase kinase 1 (MEK1) is required for Golgi fragmentation during mitosis. *J Cell Biol* 2000;149:331–339.
 28. Linstedt AD, Hauri HP. Giantin, a novel conserved Golgi membrane protein containing a cytoplasmic domain of at least 350 kDa. *Mol Biol Cell* 1993;4:679–693.
 29. Linstedt AD, Foguet M, Renz M, Seelig HP, Glick BS, Hauri HP. Sequence and overexpression of GPP130/GIMPc: evidence for saturable pH-sensitive targeting of a type II early Golgi membrane protein. *Mol Biol Cell* 1997;8:1073–1087.
 30. Schweizer A, Rohrer J, Slot JW, Geuze HJ, Kornfeld S. Reassessment of the subcellular localization of p63. *J Cell Sci* 1995;108:2477–2485.
 31. Klopfenstein DR, Klumperman J, Lustig A, Kammerer RA, Oorschot V, Hauri HP. Subdomain-specific localization of CLIMP-63 (p63) in the endoplasmic reticulum is mediated by its luminal alpha-helical segment. *J Cell Biol* 2001;153:1287–1300.
 32. Lippincott-Schwartz J, Zaal KJ. Cell cycle maintenance and biogenesis of the Golgi complex. *Histochem Cell Biol* 2000;114:93–103.
 33. Eilenberg H, Klinger E, Przeddecki F, Shechter I. Inactivation and activation of various membranal enzymes of the cholesterol biosynthetic pathway by digitonin. *J Lipid Res* 1989;30:1127–1135.
 34. Love HD, Lin CC, Short CS, Ostermann J. Isolation of functional Golgi-derived vesicles with a possible role in retrograde transport. *J Cell Biol* 1998;140:541–551.
 35. Hammond AT, Glick BS. Raising the speed limits for 4D fluorescence microscopy. *Traffic* 2000;1:935–940.
 36. Lippincott-Schwartz J, Yuan LC, Bonifacino JS, Klausner RD. Rapid redistribution of Golgi proteins into the ER in cells treated with brefeldin A. evidence for membrane cycling from Golgi to ER. *Cell* 1989;56:801–813.
 37. Lucocq JM, Pryde JG, Berger EG, Warren G. A mitotic form of the Golgi apparatus in HeLa cells. *J Cell Biol* 1987;104:865–874.
 38. Cole NB, Ellenberg J, Song J, DiEuliis D, Lippincott-Schwartz J. Retrograde transport of Golgi-localized proteins to the ER. *J Cell Biol* 1998;140:1–15.
 39. Lee TH, Linstedt AD. Osmotically induced cell volume changes alter anterograde and retrograde transport, Golgi structure, and COPI dissociation. *Mol Biol Cell* 1999;10:1445–1462.
 40. Thyberg J, Moskalewski S. Reorganization of the Golgi complex in association with mitosis: redistribution of mannosidase II to the endoplasmic reticulum and effects of brefeldin A. *J Submicrosc Cytol Pathol* 1992;24:495–508.
 41. Stein GS, Borun TW. The synthesis of acidic chromosomal proteins during the cell cycle of HeLa S-3 cells. I. The accelerated accumulation of acidic residual nuclear protein before the initiation of DNA replication. *J Cell Biol* 1972;52:292–307.
 42. Knehr M, Poppe M, Enulescu M, Eickelbaum W, Stoehr M, Schroeter D, Paweletz N. A critical appraisal of synchronization methods applied to achieve maximal enrichment of HeLa cells in specific cell cycle phases. *Exp Cell Res* 1995;217:546–553.
 43. Peterson GL. A simplification of the protein assay method of Lowry et al. which is more generally applicable. *Anal Biochem* 1977;83:346–356.
 44. Linstedt AD, Foguet M, Renz M, Seelig HP, Glick BS, Hauri HP. A C-terminally-anchored Golgi protein is inserted into the endoplasmic reticulum and then transported to the Golgi apparatus. *Proc Natl Acad Sci USA* 1995;92:5102–5105.
 45. Schweizer A, Ericsson M, Bachi T, Griffiths G, Hauri HP. Characterization of a novel 63 kDa membrane protein. Implications for the organization of the ER-to-Golgi pathway. *J Cell Sci* 1993;104:671–683.